American Mineralogist, Volume 85, pages 1485–1491, 2000

Single-crystal X-ray diffraction study of $FeGeO_3$ high-*P* clinopyroxene (*C*2/*c*) up to 8.2 GPa

T. HATTORI,[1,*] T. NAGAI,[1] T. YAMANAKA,[1] S. WERNER,[2] AND H. SCHULZ[2]

[1]Department of Earth and Space Science, Graduate School of Science, Osaka University, 1-1 Machikanayama, Toyanaka, Osaka, 560-0043, Japan

[2]Institut für Kristallographie und Angewandte, Mineralogie der Universität München, Theresienstrasse 41, D-80333 München, Germany

ABSTRACT

To elucidate pressure effects on the crystal structure of the high-*P* clinopyroxene (space group *C*2/*c*), the compression process of $FeGeO_3$ clinopyroxene (*C*2/*c*) was investigated up to 8.2 GPa by single-crystal X-ray diffraction. The crystal structure of $FeGeO_3$ is close to the ideal clinopyroxene in terms of the O atom arrangement and the tetrahedral chain configuration at ambient conditions. With pressure the lattice parameters and oxygen positions move closer to the ideal cubic closest packing (CCP) and the tetrahedral chain became more kinked with increasing pressure. However, a change in compression mechanism may occur around 4.5 GPa. All the polyhedra were homogeneously compressed above 4.5 GPa, whereas the MO_6 exhibited compressibilities 3–4 times greater than that of the TO_4 tetrahedra below 4.5 GPa. The Ge-O-Ge angle decreased with increasing pressure to 4.5 GPa and then remained constant. The close relationship between the kink angle and the relative polyhedral size suggests that this unusual compression behavior above 4.5 GPa may be caused by suppression of the extensive decrease of the Ge-O-Ge angle. The present results show that compression of pyroxenes with highly kinked tetrahedral chains is strongly effected by the kink angle.

INTRODUCTION

A high-pressure clinoenstatite (space group: *C*2/*c*) of $MgSiO_3$ was confirmed by the in-situ high pressure single crystal X-ray diffraction (Angel et al. 1992). The high-*P* clinoenstatite is believed to exist in the upper mantle. However, because this phase is stable only at high pressures above about 8 GPa (Angel et al. 1992), its compressional process of a high-*P* clinoenstatite has not been investigated by single-crystal XRD, except for measurements at one pressure (Angel et al. 1992).

Germanate pyroxenes, $MGeO_3$ (M = Co, Mn, Mg, Fe), are known to have the same structures as silicates, but at the ambient pressure (Peacor 1968; Hirano et al. 1980; Yamanaka et al. 1985) they can be considered as analogs for the silicate high-*P* clinopyroxene. The structure is based on the regular cubic closest packing (CCP) of oxygen. The tetrahedral chains are highly kinked compared with those in silicate pyroxenes, such as Ca-rich clinopyroxene (*C*2/*c*), high-temperature clinopyroxene (*C*2/*c*), orthoenstatite (*Pbca*) and low-clinoenstatite ($P2_1/c$) (Cameron and Papike 1980). The kink is clearly shown by the small O3-O3-O3 angle, where O3 is the bridging oxygen of the tetrahedra. The kink angles of germanate clinopyroxenes (*C*2/*c*) are close to 120° for the ideal structure (Thompson 1970) and are smaller for all pyroxenes. The M1 and M2 octahedra in the high-*P* pyroxene are very regular compared with those of the above mentioned other pyroxenes. The germanate clinopyroxenes (*C*2/*c*) are often compared to the ideal clinopyroxene structure in terms of the above mentioned characteristics (Papike et al. 1973).

Previous results on pyroxenes (Levien and Prewitt 1981; Zhang et al. 1997; Hugh-Jones and Angel 1994; Hugh-Jones et al. 1997) suggest that compression of pyroxenes is mainly controlled by compression of the soft octahedra rather than the rigid tetrahedra. The tetrahedra only rotate to accommodate the octahedral bands. Consequently, the tetrahedral chains become more kinked with increasing pressure. Structure refinement results show that the O3-O3-O3 angles of the germanate and silicate high-*P* clinopyroxenes (*C*2/*c*) are 129.03° for $MgGeO_3$ and 131.1° for $FeGeO_3$ at ambient pressure, and 133.4° for $MgSiO_3$ at 7.94 GPa and 138.4° for $FeSiO_3$ at 1.84 GPa (Yamanaka et al. 1985; Yamanaka, personal communication; Hugh-Jones and Angel 1994; Hugh-Jones et al. 1997).

In the present study, single crystal X-ray diffraction was carried out on $FeGeO_3$ clinopyroxene up to 8.2 GPa to reveal the compression process of high-*P* clinopyroxene and to comprehend the structure of high-*P* clinopyroxene at higher pressure above 8 GPa.

EXPERIMENTAL METHODS

Sample preparation

The specimen was synthesized after Takayama and Kimizuka (1981). Reagent-grade powders in molar ratio of $Fe:Fe_2O_3:GeO_2 = 1:1:3$ were mixed homogeneously by mortar and formed into pellets. They were sealed in evacuated silica

* Present address: Department of Physics, Faculty of Science and Technology, Keio University 3-14-1, Hiyoshi-ku, Yokohama 223-8522 Japan
E-mail: takanori@phys.keio.ac.jp

tubes and heated at 1000 °C for 14 days. The single crystals with the linear sizes of ~100 μm were obtained. Electron microprobe analyses showed that the synthetic sample had the chemical composition of $FeGeO_3$ within the experimental uncertainty. The space group of *C2/c* was confirmed by the precession photographs. Single-crystals free from twins or optical imperfections were selected for intensity measurements. One single-crystal with dimensions of $140 \times 110 \times 105$ μm^3 was used for structure refinement at ambient pressure. Another single crystal with about $80 \times 80 \times 40$ μm^3 was used for structure refinements at high pressures.

High-pressure X-ray diffraction technique

The single crystal experiment at ambient condition was carried without the diamond anvil cell (DAC) on Rigaku-AFC5 4-circle diffractometer at Yamanaka laboratory at Osaka University. High-pressure experiments were carried in the DAC on a Nonius CAD4 κ-type diffractometer at München University. The X-rays were generated by a Mo sealed tube and monochromatized by a pyrolytic graphite.

A modified Merrill-Bassett DAC, which was developed by the München group, was used in the high-pressure experiments (Werner et al. 1996). A pair of diamonds with the culet sizes of 400 μm and 600 μm was used. The diamonds were supported by the beryllium backing plates. In the high-pressure experiment, the single crystal was sealed in the gasket hole together with pressure marker (ruby chips) and the pressure transmitting medium (a mixture of methanol and ethanol in volume ratio of 4:1). A spring steel gasket was preindented to 80 μm in thickness beforehand, and a hole of 250 μm was made in the center of the gasket by a spark erosion system. The applied pressure on the sample was measured by the ruby fluorescence method (Mao et al. 1986).

In the high-pressure experiments, it was difficult to put the sample in DAC on the cross center of the goniometer by optical microscope because of apparent shift of the image of the sample due to differences of the refractive indexes between diamond and air. Therefore, the sample in DAC was set to the center by checking the profile of the direct beam through the gasket hole (Primary beam profile method, Werner et al. 1996). This method allows location of the crystal in the center within an accuracy of 30 μm. Lattice parameters were determined from the positions of more than 20 reflections with $2\theta > 20°$ by employing least squares refinements. Each reflection was centered at four equivalent positions to reduce systematic errors which were introduced by the misalignment of the sample crystal on the diffractometer.

Intensity data collection and data reduction

Intensity data were collected at five pressure points (experimental conditions are in Table 1). The intensity data for the sample at ambient pressure were collected by using the ω-scanning mode at the bisecting positions.

For the high-pressure experiments, the X-ray diffraction intensities were measured at phi-fixed position ($\phi = 0°$) (Finger and King 1978), using the ω-scanning mode to reduce effects of the Debye-Scherrer rings from beryllium or gasket. For data collection at 7.4 GPa, the diffraction intensities were also measured at two different ψ positions ($\psi = \pm 0.2°$) to reduce errors caused by "dips," originating from the diamonds (Loveday et al. 1990). The X-ray diffraction intensities were measured up to 2θ near 67°. All diffraction peak profiles were checked in terms of the background height and the consistency of diffraction intensities among the equivalent reflections. The data reduction utilized REDA, a program developed by Munchen group for special purposes of high-pressure structure analysis. The absorption correction of the diffraction intensities by the diamonds and beryllium backing plates were determined by measuring transparency of the direct beam as a function of inclination of the DAC. Raw intensity data were corrected for this X-ray absorption and Lorentz-polarization factor. The correction of the absorption by sample itself was negligibly small. Diffraction intensities were integrated after these corrections.

Structure refinement

Reflections with structure factors of $|F_o| > 6\ \sigma(|F_o|)$ were used for structure refinements. Full matrix least-squares refinements were conducted by using the program RADY (Sasaki 1987). Atomic scattering factors and anomalous dispersion parameters were taken from the *International table for X-ray Crystallography* (Ibers and Hamilton 1974). The lattice parameters, number of the reflections used for refinements and the final residuals, *R* and *wR* are listed in Table 1. The atomic coordinates at various pressures are in Table 2. Interatomic distances, polyhedral volumes and distortion parameters for the polyhedra, edge distance ratios of polyhedra and the tetrahedral chain angles are in Table 3. The uncertainties (estimated standard deviations, e.s.d.s) of the calculated parameters, such as polyhedral volumes and chain angles were estimated on the basis of the error propagation of those in the lattice parameters and atomic positions.

RESULTS

Oxygen packing

In the clinopyroxene *C2/c* structure, the lattice parameters are closely related to the oxygen arrangement. The calculated lattice parameters of the ideal pyroxene with the complete CCP of oxygen are in Table 1. The relative differences between the observed and ideal lattice parameters at 1 atm are $a = 5.51\%$, $b = 8.81\%$, $c = 7.32\%$, and $\beta = 1.77\%$. $FeGeO_3$ clinopyroxene has the largest deviation along the *b*-axis compared to the ideal clinopyroxene at ambient pressure. With increasing pressure, the *b*-axis is most largely compressed (Fig. 1). The linear compressibilities of the three axes are $\beta = 0.00262(11)$/GPa, $\beta_b = 0.00343(11)$/GPa and $\beta_c = 0.00242(18)$/GPa, respectively. The axial ratios of *a/b*, and *c/b* increase and approach to those of the ideal clinopyroxene. The β-angle decreases continuously toward 100.025°, the value of the ideal clinopyroxene. These imply that the oxygen packing approaches toward the ideal CCP with increasing pressure. The change of the lattice parameters is well consistent with the results of the powder diffraction (Hattori et al. 1999).

To confirm the inference that the oxygen arrangement approaches to the ideal CCP from the point of atomic positions, the observed atomic positions of O atoms are compared with

TABLE 1. Lattice parameters (Å) and the factors of refinements

Pressure (GPa)	10^{-4}	1.5	2.9	4.1	4.5	5.4	6.0	7.4	8.2	Ideal *	
a (Å)	9.798(2)	9.746(1)	9.714(7)	9.682(6)	9.651(5)	9.649(10)	9.636(4)	9.600(5)	9.583(3)	2 √11r	= 9.287
b (Å)	9.140(1)	9.084(1)	9.043(3)	9.014(1)	8.988(1)	8.962(4)	8.946(1)	8.912(1)	8.883(3)	6r	= 8.400
c (Å)	5.205(1)	5.177(1)	5.156(6)	5.141(2)	5.136(1)	5.110(3)	5.119(1)	5.108(1)	5.093(2)	2√3r	= 4.850
β (°)	101.80(1)	101.52(2)	101.27(1)	101.11(5)	100.97(2)	100.85(10)	100.82(2)	100.67(2)	100.56(4)	$\tan^{-1}(-4\sqrt{2})$	= 100.025
a/*b*	1.072	1.073	1.074	1.074	1.074	1.077	1.077	1.077	1.079	√11/3	= 1.1055
c/*b*	0.569	0.570	0.570	0.570	0.571	0.570	0.572	0.573	0.573	1/√3	= 0.5774
V (Å^3)	456.3(1)	449.1(1)	444.2(6)	440.3(3)	437.3(3)	434.0(6)	433.4(2)	429.5(2)	426.2(2)	96√2r^3	= 372.54
(A, B)†	(1.30, 0.35)	(0.61, 0.47)	–	–	(0.61, 0.47)		–	–	(0.61, 0.47)	(0.61, 0.47)	–
2θ range (°)	117.6	67.6	–	–	63.3	–	–	67.9	63.4	–	
No. of reflections	2763	1083	–	–	978	–	–	2821	957	–	
No. of reflections ‡	1145	274	–	–	253	–	–	232	303	–	
R (%)	5.77	6.67	–	–	5.57	–	–	5.11	6.93	–	
wR (%)	5.97	8.02	–	–	7.06	–	–	5.16	6.19	–	

Notes: Weighting scheme is $1/\sigma^2(|F_o|)$.
* Ionic radius of oxygen [r (O) = 140 Å] is based on Shannon (1976).
† Scan width, Δω (°) = A + B tanθ.
‡ After averaging with $|F_o| > 6\ \sigma(|F_o|)$.

TABLE 2. Atomic coordinates of the observed and ideal pyroxenes

		0 GPa	1.5 GPa	4.5 GPa	7.4 GPa	8.2 GPa	Ideal
Fe1	*x*	0.0	0.0	0.0	0.0	0.0	0.0
	y	0.9076(1)	0.9084(3)	0.9101(3)	0.9111(3)	0.9115(2)	11/12
	z	0.25	0.25	0.25	0.25	0.25	1/4
	B_{eq}	0.56(1)	1.48(5)	1.43(5)	1.49(4)	1.32(4)	
Fe2	*x*	0.0	0.0	0.0	0.0	0.0	0.0
	y	0.2709(1)	0.2715(3)	0.2723(3)	0.2727(3)	0.2728(2)	1/4
	z	0.25	0.25	0.25	0.25	0.25	1/4
	B_{eq}	0.54(1)	1.45(6)	1.38(6)	1.48(5)	1.26(4)	
Ge	*x*	0.3006(1)	0.3011(4)	0.3015(3)	0.3023(3)	0.3022(3)	5/16
	y	0.0925(1)	0.0927(2)	0.0936(2)	0.0941(2)	0.0943(1)	1/12
	z	0.2161(1)	0.2155(3)	0.2145(3)	0.2138(2)	0.2136(2)	3/16
	B_{eq}	0.362(6)	1.38(4)	1.27(4)	1.41(3)	1.27(3)	
O1	*x*	0.1186(3)	0.1193(22)	0.1181(23)	0.1193(20)	0.1197(17)	1/8
	y	0.0899(4)	0.0891(9)	0.0910(10)	0.0910(9)	0.0898(7)	1/12
	z	0.1388(6)	0.1366(18)	0.1350(18)	0.1360(15)	0.1340(15)	1/8
	B_{eq}	0.54(4)	1.52(18)	1.37(17)	1.39(14)	1.49(14)	
O2	*x*	0.3840(4)	0.3875(21)	0.3860(23)	0.3806(21)	0.3820(16)	3/8
	y	0.2402(4)	0.2418(11)	0.2440(10)	0.2465(10)	0.2463(8)	1/4
	z	0.3833(7)	0.3845(18)	0.3879(18)	0.3867(17)	0.3848(14)	3/8
	B_{eq}	0.58(5)	1.87(20)	1.47(17)	1.67(16)	1.63(14)	
O3	*x*	0.3583(4)	0.3601(24)	0.3645(22)	0.3654(21)	0.3629(15)	3/8
	y	0.0647(4)	0.0661(10)	0.0657(10)	0.0656(9)	0.0680(7)	1/12
	z	0.9161(7)	0.9127(20)	0.9134(19)	0.9098(17)	0.9081(14)	7/8
	B_{eq}	0.58(5)	1.57(19)	1.44(18)	1.63(17)	1.37(14)	

those of the ideal CCP. The atomic coordinates of the ideal clinopyroxene in Table 2, are based on the rigid oxygen packing model. The deviation of the oxygen arrangement from the ideal CCP can be represented by the sums of root squares of displacements of the crystallographically independent O atoms, O1, O2, O3, from their ideal positions. The deviations are expressed in terms of the three directions of (1) along an arbitrary direction (total), (2) along the stacking direction *(//a*)* and (3) within an oxygen stacking layer (*b*-*c* plane) by the following equations:

$$D_{\text{total}} = \frac{1}{3}\sum_{i=1}^{3}\sqrt{(a\Delta x_i)^2 + (b\Delta y_i)^2 + (c\Delta z_i)^2}$$

$$D_{//a^*} = \frac{1}{3}\sum_{i=1}^{3}\sqrt{(a\Delta x_i)^2}$$

$$D_{b-c} = \frac{1}{3}\sum_{i=1}^{3}\sqrt{(b\Delta y_i)^2 + (c\Delta z_i)^2}$$

where Δx_i, Δy_i, and Δz_i are the differences of the *x*, *y,* and *z* coordinates for the *i* th oxygen between the observed and ideal structures, respectively. All the deviation parameters are equal

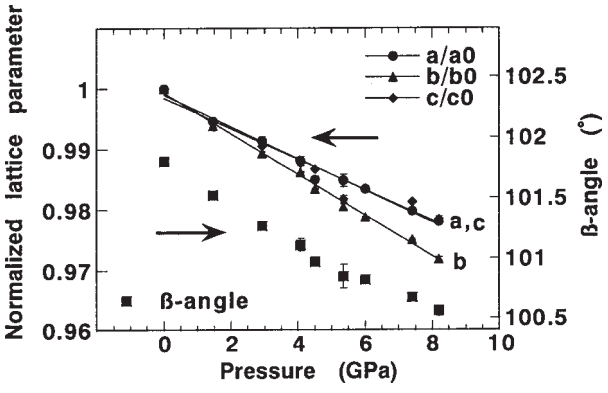

FIGURE 1. Normalized lattice parameters at high pressure. Error bars = estimated standard deviations. The normalized lattice parameters are fitted linearly.

TABLE 3. Interatomic distances (Å), polyhedral volumes (Å^3), and the distortion parameters for polyhedra, the edge distance ratios of polyhedra and tetrahedral chain angles (°)

Pressure (GPa)	10^{-4}	1.5	4.5	7.4	8.2
Fe1-O1(1, 2)*	2.176(4)	2.159(16)	2.133(17)	2.114(15)	2.103(17)
Fe1-O1(3, 4)	2.117(3)	2.104(22)	2.086(25)	2.089(26)	2.078(44)
Fe1-O2(5, 6)	2.107(4)	2.070(16)	2.058(17)	2.062(17)	2.047(19)
Mean Fe1-O	2.133(3)	2.111(18)	2.092(20)	2.088(19)	2.076(27)
Mean O-O	3.014(4)	2.977(25)	2.956(28)	2.937(27)	2.934(38)
Volume	12.79(3)	12.39(18)	12.06(19)	12.04(17)	11.84(14)
Q.E	1.0086(2)	1.0084(15)	1.0085(16)	1.0057(14)	1.0050(12)
A.V	28.5(8)	27.8(51)	28.4(54)	19.3(48)	17.0(40)
Fe2-O1(1, 2)	2.168(4)	2.171(16)	2.135(17)	2.126(15)	2.134(17)
Fe2-O2(7, 8)	2.014(3)	1.993(21)	1.978(25)	2.000(27)	1.999(43)
Fe2-O3(7, 8)	2.329(4)	2.281(19)	2.225(19)	2.192(19)	2.183(22)
Mean Fe2-O	2.170(4)	2.148(19)	2.113(20)	2.106(20)	2.105(27)
Mean O-O	3.069(6)	3.036(27)	2.985(28)	2.981(28)	2.972(38)
Volume	13.41(4)	12.99(16)	12.37(16)	12.28(14)	12.27(11)
Q.E	1.0145(3)	1.0149(12)	1.0135(13)	1.0105(12)	1.0109(9)
A.V	29.7(7)	32.8(29)	32.6(31)	28.1(27)	29.7(22)
Ge-O1(1)	1.746(3)	1.738(23)	1.739(23)	1.728(21)	1.722(23)
Ge-O2(1)	1.720(3)	1.736(14)	1.735(15)	1.715(14)	1.710(18)
Ge-O3(1)	1.784(4)	1.790(18)	1.784(18)	1.787(17)	1.774(23)
Ge-O3(4)	1.797(3)	1.794(12)	1.796(12)	1.780(12)	1.784(15)
Mean Ge-O	1.762(3)	1.765(16)	1.764(17)	1.753(16)	1.748(20)
Mean O-O	2.872(5)	2.876(26)	2.874(28)	2.863(26)	2.848(33)
Volume	2.782(7)	2.792(35)	2.785(35)	2.742(32)	2.716(26)
Q.E	1.0058(2)	1.0069(6)	1.0069(7)	1.0056(6)	1.0059(5)
A.V	25.4(7)	30.9(28)	30.5(30)	24.2(27)	26.2(21)
Void space (Å^3)	329.2	325.2	317.3	310.3	308.1
d_{tet}/d_{oct} †	0.944(2)	0.957(12)	0.967(13)	0.967(13)	0.965(17)
O3-O3-O3‡	131.1(3)	130.2(7)	130.6(7)	130.8(6)	129.3(5)
Ge-O3-Ge‡	120.1(2)	119.0(10)	117.9(9)	117.9(9)	117.9(7)
Tilting angle§	5.8	6.1	4.8	3.3	4.2

Note: Standard deviations are given in parentheses. QE= quadratic elongation for each polyhedra (Robinson et al. 1971). AV= angle variance for each polyhedra (Robinson et al. 1971).
* Symmetry operation for each oxygen is shown in the parentheses.
† The edge distance ratio of polyhedra is d_{tet}/d_{oct}= O-O_{tet}/[(O-O_{M1oct}+ O-O_{M2oct})/2].
‡ Tetrahedral chain angles.
§ Angle between the normals of basal plane of a tetrahedron and of the *b-c* plane.

to zero when the oxygen arrangement becomes complete CCP. The β-angle is not considered in the above equations, because its effects on the deviations is found to be negligibly small. All the deviation parameters (Table 4) decrease with pressure. No remarkable differences in the three directions are observed. These results confirms that the O atoms shift their positions toward those of CCP under pressure. Completion of the oxygen arrangement to the CCP is not observed within the pressure range up to 8.2 GPa.

Compression of polyhedra

Normalized volumes of the polyhedra, void space and unit cell (Fig. 2) suggest that the compression process may be divided into two stages below and above 4.5 GPa, in terms of polyhedral volume compressibilities. Volume compressibilities of these polyhedra are $\beta_v[M1O_6] = 0.0134(27)$/GPa, $\beta_v[M2O_6] = 0.0175(13)$/GPa, and $\beta_v[TO_4] = -0.00055(50)$/GPa below 4.5 GPa. M1 and M2 octahedra are about 3 times more compressible than the tetrahedron. No significant compression of the tetrahedron is not observed. This compressional behavior has been observed in many pyroxenes (Levien and Prewitt 1981; Zhang et al. 1997).

The compressibilities for the polyhedra are $\beta_v[M1O_6] = 0.0042(36)$/GPa, $\beta_v[M2O_6] = 0.0021(1)$/GPa and $\beta_v[TO_4] =$

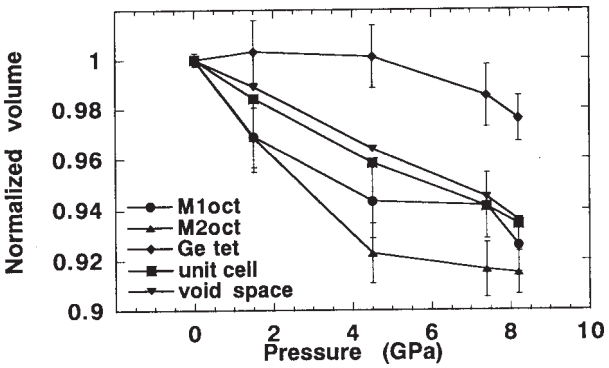

FIGURE 2. Normalized volumes of the polyhedra, void space and unit cell. Error bars = estimated standard deviations.

TABLE 4. Deviation parameters (Å) of the oxygen arrangement in the three directions along an arbitrary direction (total), along the stacking direction (*//a**) and within an oxygen stacking layer (*b-c* plane)

	Pressure(GPa)					
	10^{-4}	1.5	4.5	7.4	8.2	Ideal
D_{total}	0.188(1)	0.179(3)	0.173(3)	0.148(2)	0.142(2)	0.0
$D_{//a^*}$	0.105(1)	0.107(5)	0.092(4)	0.067(4)	0.078(3)	0.0
$D_{b\text{-}c}$	0.155(1)	0.140(2)	0.141(2)	0.131(2)	0.117(2)	0.0

0.0066(11)/GPa between 4.5 GPa and 8.2 GPa. The difference of the volume compressibility of tetrahedron at high and low P is more than 3 $\sigma(\beta_v\,[TO_4])|_{4.5<P<8.2}$, where $\sigma(\beta_v\,[TO_4])|_{4.5<P<8.2}$ is the e.s.d.s of the compressibility of TO_4 tetrahedra between 4.5 and 8.2 GPa. This indicates a change in compression behavior at 4.5 GPa. In this pressure range, the GeO_4 tetrahedra are compressed by 2.4% relative to their room pressure volume. The amount corresponds to 2.5 $\sigma(V)|_{P=8.2GPa}$. This compression is therefore significant. The compressibility of the GeO_4 tetrahedron is similar to that of $MgGeO_3$ clinopyroxene ($C2/c$) ($\beta_v\,[GeO_4]$ = 0.0074/GPa) determined by EXAFS (Andrault et al. 1992). On the other hand, the compressibility of M1 and M2 octahedra above 4.5 GPa are smaller than those below 4.5 GPa. The tetrahedra are as compressible as, or more compressible than, the octahedra in this pressure region. On the other hand, through the whole pressure region, void space and unit cell are compressed linearly.

Deformation of polyhedra

Below 4.5 GPa, the M-O bonds in each M1 and M2 octahedron shorten at similar rates with increasing pressure. Quadratic elongations (QE) and angle variances (AV) of M1 and M2 octahedra are almost constant with increasing pressure. The changes of quadratic elongations of M1 and M2 octahedra are within 0.13 $\sigma(QE)|_{P=4.5GPa}$ and 1.1 $\sigma(QE)|_{P=4.5GPa}$, respectively. On the other hand, the longer M-O bonds decrease continuously and the shorter M-O bonds remain constant with increasing pressure between 4.5 and 8.2 GPa within each octahedron. Consequently, the M-O bonds in each octahedron become more equal distance. The quadratic elongation and angle variance in both M1 and M2 octahedra decrease with pressure below 4.5 GPa. The decrease of the quadratic elongations of M1 and M2 octahedra are respectively 2.9 $\sigma(Q.E)|_{P=8.2GPa}$ and 1.6 $\sigma(Q.E)|_{P=8.2GPa}$. These observations show that the M1 and M2 octahedra become more regular above 4.5 GPa.

No significant change of the tetrahedral dimension is observed below 4.5 GPa. Above 4.5 GPa, all the T-O bonds start to decrease at similar rates without deformation of the tetrahedron.

In summary, the M1 and M2 octahedra are compressed by decrease of all M-O bonds below 4.5 GPa and are compressed by polyhedral deformation toward more regular octahedra above 4.5 GPa. On the other hand, the tetrahedra do not show any change below 4.5 GPa and are compressed isotropically by shortening all the T-O bonds above 4.5 GPa.

Tetrahedral chain configuration

The kink of the tetrahedral chain is represented by the O3-O3-O3 angle (Fig. 3a), and the tilt of a tetrahedron by the angle between the normals of the basal plane of the tetrahedron and the *b-c* plane (Fig. 3b). At the ambient pressure, the O3-O3-O3 angle (131.1°) and the tilt angle (5.8°) are slightly deviated from their respective values of 120° and 0° of the ideal clinopyroxene structure. With increasing pressure, the O3-O3-O3 angle and tilt angle decrease, respectively, to 129.3° at a rate of –0.11(9)°/GPa and 4.2° at a rate of –0.29(8)°/GPa. No kink point is observed in both curves within experimental uncertainty. The tetrahedral chain kinks more significantly and approaches to the ideal configuration with increasing pressure. The completely ideal configuration is not observed within the pressure range of the present study.

The Ge-O-Ge angle is measured across the neighboring tetrahedra through the bridging oxygen (Fig. 3). The angle is 120.1° at ambient pressure and is significantly deviated from the ideal angle of 109.5°. Below 4.5 GPa, the Ge-O-Ge angle decreases smoothly to 117.9° with increasing pressure. Above 4.5 GPa, the Ge-O-Ge angle remains constant but do not approach the ideal angle (Fig. 4).

DISCUSSION

Compression behavior below 4.5 GPa

The edge distance ratio (Table 3 and Fig. 5)increases with pressure below 4.5 GPa. This may be caused by the preferential compression of the octahedra. Based on Thompson's model of the ideal pyroxene structure (1970), where the polyhedra are completely regular and the base of individual polyhedra is parallel to the *b-c* plane, the following relation holds between the edge distance ratio, d_{tet}/d_{oct}, and the O3-O3-O3 angle (Fig. 3a).

$$\angle O3-O3-O3 = 2\sin^{-1}\left[\frac{\sqrt{3}}{2}\left(\frac{d_{tet}}{d_{oct}}\right)^{-1}\right] \qquad (4)$$

According to this relation, an increase in the edge distance ratio leads to a decrease in the O3-O3-O3 angle. The observed kinking of tetrahedral chain appears to be caused by the increase of the edge distance ratio due to the preferential compression of octahedra below 4.5 GPa.

The tilting of tetrahedron out of the *b-c* plane can be similarly explained. The projection view of the clinopyroxene structure along the *c*-direction helps understand the nature of the tetrahedral tilting (Fig. 3b). Two factors are responsible for decreasing the tilt angle. One is an increase in the edge distance ratio and the other is deformation of the M1 and M2 octahedra. In the present study, the latter seems to have little effect on the tilt angle because significant deformation of the M1 and M2 octahedra is not observed below 4.5 GPa. Assuming that the polyhedra are completely regular and the tetrahedra are fully rotated in the *b-c* plane, the relation between the edge distance ratio, d_{tet}/d_{oct} and tilt angle, θ_{tilt} can be expressed as follows (Fig. 3b):

$$4\sqrt{\frac{2}{3}}\sin\theta_{tilt} + \cos\theta_{tilt} = \left(\frac{d_{tet}}{d_{oct}}\right)^{-1} \qquad (5)$$

This equation shows that an increase in the edge distance ratio will give rise to a decrease in the tilt angle. This observed tilting of the tetrahedra can be understood by the increase of the edge distance ratio of polyhedra.

All the observed changes in the tetrahedral configuration and oxygen arrangement below 4.5 GPa can be interpreted by the preferential compression of the octahedra. The kinking of tetrahedral chain and the rotation of tetrahedra make the oxygen packing regular. Consequently, we conclude that the compression behavior below 4.5 GPa is mainly controlled by individual compressibilities of polyhedra.

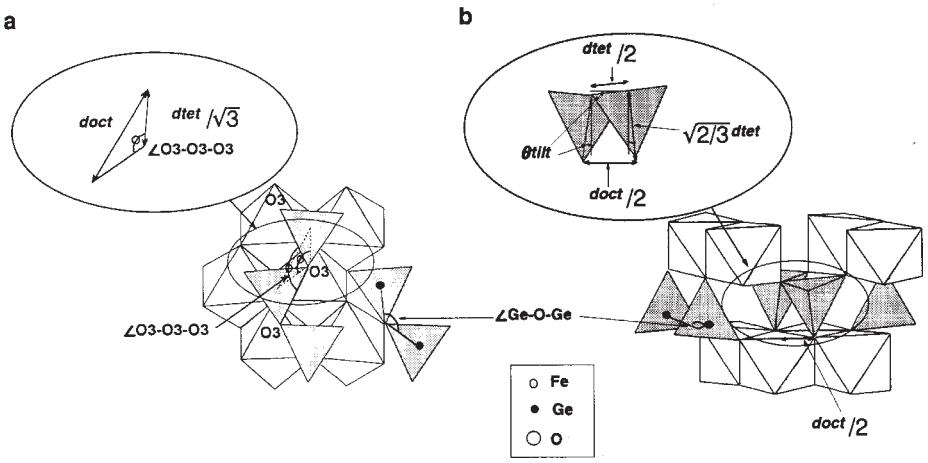

FIGURE 3. Projections of the high-*P* clinopyroxene (*C2/c*) structure (**a**) onto the *b*-*c* plane and (**b**) along *c* direction. GeO_4 tetrahedron are shaded; FeO_6 octahedron are open.

Compression behavior above 4.5 GPa

The polyhedra are homogeneously compressed above 4.5 GPa, and the edge distance ratio remains constant (Fig. 5). This compression behavior is different from that below 4.5 GPa. Polyhedral compressibilities can be estimated from their empirical relations to the polyhedral charge densities (Hazen and Prewitt 1977). The estimated compressibilities of the respective polyhedra are $\beta_v[M1O_6] = 0.0054$ GPa^{-1}, $\beta_v[M2O_6] = 0.0057$ GPa^{-1} and $\beta_v[TO_4] = 0.0015$ GPa^{-1} at 4.5 GPa. These values suggest that the octahedra are more compressible than tetrahedra even at 4.5 GPa and, therefore, the preferential compression of the octahedra should continue over 4.5 GPa. However, the observed compressibilities of octahedra are smaller, and the tetrahedra larger, than the estimated values. Thus, above empirical relationship does not seem to be applicable to the compression process above 4.5 GPa. The relationship was established based mainly on compression data of simple oxides (Hazen and Prewitt 1977). The interaction between the metal cation and its first neighbor oxygen would play a main role in compression of polyhedra in these oxides. However, the compression of octahedra in high-*P* clinopyroxene seems to be controlled not only by the above interaction but also the flexibility of the tetrahedral chain. The presently observed cessation of decrease in Ge-O-Ge angle at 4.5 GPa supports this idea.

Gibbs et al. (1987) have calculated the total energy of H_6Ge_2O molecules as a function of Ge-O bond length and Ge-O-Ge bond angle by molecular orbital (MO) calculation. The molecule has an energy potential minimum at a Ge-O-Ge bond angle of 133.4° and Ge-O bond distance of 1.756 Å. If this result can be applied to $FeGeO_3$ high-*P* clinopyroxene, then the presently observed decrease of Ge-O-Ge angle from 120.1° to 117.9° below 4.5 GPa would contribute to the instability of the tetrahedral chain. It is considered from the calculated potential curve of the Ge-O-Ge angle that further kinking of the tetrahedral chain would be unfavorable in terms of local energy of the Ge-O-Ge linkage. In the pressure range above 4.5 GPa, both octahedra and tetrahedra would be compressed at similar rates to avoid further decrease of the Ge-O-Ge angle. These arguments suggest that compression of high-*P* clinopyroxene above 4.5 GPa is strongly affected by the kink of tetrahedral chain as well as the compressibilities of the polyhedra.

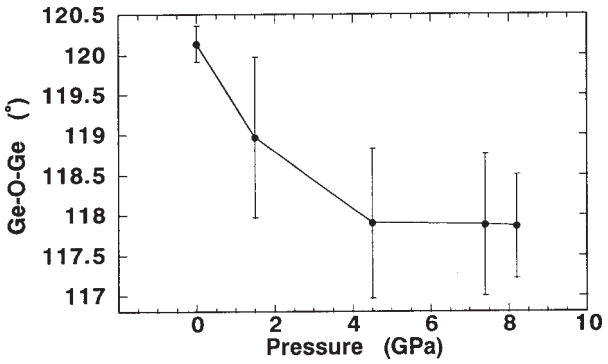

FIGURE 4. Ge-O-Ge angles at high pressures.

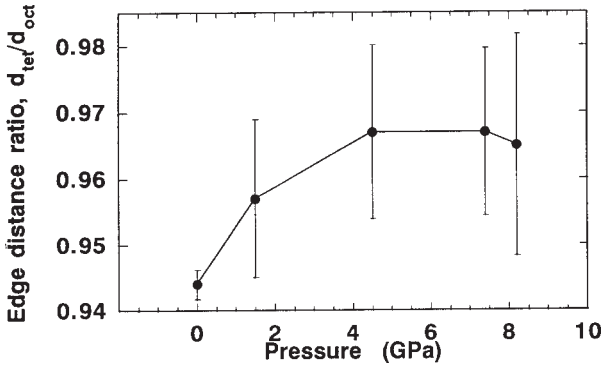

FIGURE 5. Edge distance ratio, d_{tet}/d_{oct}, of polyhedra at high pressures. See Table 3.

Unusual compression of polyhedra in silicate pyroxenes

Hugh-Jones and Angel (1994), and Hugh-Jones et al. (1997) investigated the compression behavior of $MgSiO_3$ and $(Mg,Fe)SiO_3$ orthoenstatites (*Pbca*), respectively. Both orthoenstatites changes the compressional mechanisms at about 4 GPa. Below 4 GPa, the SiO_4 tetrahedra are essentially incompressible with no

change in Si-O bond length, whereas the tetrahedra are significantly compressed with shortening of Si-O bond above the pressure. The tetrahedral chains also change the kink mode at 4 GPa: the B-chains (<O3B-O3B-O3B = 139° for $MgSiO_3$, 141.9° for $(Mg,Fe)SiO_3$), which is kinked more compared to the A chain, kink dramatically with increasing pressure up to 4 GPa, and the kinking ceases at about 4 GPa. These results show that the main compression mechanism of the orthoenstatites change from the bending of tetrahedral chain into the shortening of Si-O bond at 4 GPa which is the boundary pressure of the compression mechanism. Our results of the compression on $FeGeO_3$ clinopyroxene are similar to the above compression behavior of the orthoenstatites. From the viewpoints of the crystal structure, silicate orthoenstatites and $FeGeO_3$ clinopyroxene have the highly kinked tetrahedral chain in common. Present study on $FeGeO_3$ suggests that the compression mechanism may be induced from the avoidance of the high kinking of tetrahedral chain. Judging from the structural similarity in the tetrahedral chain configuration between orthoenstatite and $FeGeO_3$ clinopyroxene, it is considered that the change of the compression behavior in orthoenstatites would be induced from the avoidance of the kink of the SiO_4 tetrahedral chain.

ACKNOWLEDGMENTS

The authors thank P. Dreier for the technical support of the data collection and G. Yagyu for the assistance of the sample preparation. We also thank R. Thompson and an anonymous reviewer for their helpful comments and Y. Wang for improving the manuscript. This work was supported by the Grant-in-Aid for International Scientific Research, Ministry of Education, Science and Culture (grant no. 08044082).

REFERENCES CITED

Andrault, D., Madon, M., Itie, J.P., and Fontaine, A. (1992) Compression and coordination changes in pyroxenoids: an EXAFS study of $MgGeO_3$ enstatite and $CaGeO_3$ wollastonite. Physics and Chemistry of Minerals, 18, 506–513.

Angel, R.J., Chopelas, A., and Ross, N.L. (1992) Stability of high-density clinoenstatite at upper-mantle pressures. Nature, 358, 322–324.

Cameron, M. and Papike, J.J. (1980) Crystal chemistry of silicate pyroxenes. In Mineralogical Society of America Reviews in Mineralogy, 7, 5–92.

Finger, L.W. and King, H. (1978) A revised method of operation of the single-crystal diamond cell and refinement of the structure of NaCl at 32 kbar. American Mineralogist, 63, 337–342.

Gibbs, G.V., D'Arco, P., and Boisen, M.B. (1987) Molecular mimicry of bond length and angle variations in germanate and thiogermanate crystals: A comparison with variations calculated for C-, Si-, and Sn-containing oxide and sulfide molecules. The Journal of Physical Chemistry, 91, 5347–5354.

Hattori, T., Matsuda, T., Tsuchiya, T., Nagai, T., and Yamanaka, T. (1999) Clinopyroxene-perovskite phase transition of $FeGeO_3$ under high pressure and room temperature. Physics and Chemistry of Minerals, 26, 212–216.

Hazen, R.M. and Prewitt, C.T. (1977) Effects of temperature and pressure on interatomic distances in oxygen-based minerals. American Mineralogist, 62, 309–315.

Hirano, M., Tokonami, M., and Morimoto, N. (1980) Crystal chemistry of $MnGeO_3$ polymorphs. Journal of Mineralogical Society of Japan, 14, 158–164.

Hugh-Jones, D.A. and Angel, R.J. (1994) A compressional study of $MgSiO_3$ orthoenstatite up to 8.5 GPa. American Mineralogist, 79, 405–410.

Hugh-Jones, D.A., Chopelas, A., and Angel, R.J. (1997) Tetrahedral compression in $(Mg, Fe)SiO_3$ orthopyroxenes. Physics and Chemistry of Minerals, 24, 301–310.

Ibers, J.A. and Hamilton, W.C., Eds. (1974) International tables for X-ray crystallography, vol. IV, 366 p. Kynoch, Birmingham, U.K.

Levien, L. and Prewitt, C.T. (1981) High-pressure structural study of diopside. American Mineralogist, 66, 315–323.

Loveday, J.S., McMahon, M.I., and Nelmes, R.J. (1990) The effect of diffraction by the diamonds of a diamond-anvil cell on single-crystal sample intensities. Journal of Applied Crystallography, 23, 392–396.

Mao, H.K., Xu, J., and Bell, P.M. (1986) Calibration of the ruby pressure gauge to 800 kbar under quasi-hydrostatic condition. Journal of Geophysical Research, 91, 4673–4676.

Papike, J.J., Prewitt, C.T., Sueno, S., and Cameron, M. (1973) Pyroxenes: comparisons of real and ideal structural topologies. Zeitschrift fur Kristallographie, 138, 254–273.

Peacor, D.R. (1968) The crystal structure of $CoGeO_3$. Zeitschrift für Kristallographie, 126, 299–306.

Robinson, K. Gibbs, G.V., and Ribbe, P.H. (1971) Quadratic elongation: a quantitative measure of distortion in coordination polyhedra. Science, 172, 567–570.

Sasaki, S. (1987) RADY: A fortran program for the least-squares refinement of crystal structures, KEK internal 87–3, Tsukuba, National laboratory for high energy physics.

Shannon, R.D. (1976) Revised effective ionic radii and systematic studies of interatomic distances in halides and chalcogenides. Acta Crystllographica, A32, 751–767.

Takayama, E. and Kimizuka, N. (1981) Powder X-ray study on iron-germanium pyroxenes. Journal of Solid State Chememistry 39, 262–264.

Thompson, J.B. (1970) Geometrical possibilities for amphibole structures: model biopyriboles. American Mineralogist, 55, 292–293.

Werner, S., Kim-Zajonz, J., Wittlinger, J., and Schulz, H. (1996) Workshop on the Use of ultrashort Wavelengths. Hasylab, Hamburg, Germany (Proceedings).

Yamanaka, T., Hirano, M., and Takeuchi, Y. (1985) A high temperature transition in $MgGeO_3$ from clinopyroxene (*C2/c*) type to orthopyroxene (*Pbca*) type. American Mineralogist, 70, 365–374.

Zhang, Li., Ahsbahs, H., Hafner, S.S., and Kutoglu, A. (1997) Single-crystal compression and crystal structure of clinopyroxene up to 10 GPa. American Mineralogist, 82, 245–258.

MANUSCRIPT RECEIVED AUGUST 23, 1999
MANUSCRIPT ACCEPTED MAY 2, 2000
PAPER HANDLED BY YANBIN WANG